

# The interior of a binary black hole merger

Daniel Pook-Kolb,<sup>1,2</sup> Ofek Birnholtz,<sup>3</sup> Badri Krishnan,<sup>1,2</sup> and Erik Schnetter<sup>4,5,6</sup>

<sup>1</sup>*Max-Planck-Institut für Gravitationsphysik (Albert Einstein Institute), Callinstr. 38, 30167 Hannover, Germany*

<sup>2</sup>*Leibniz Universität Hannover, 30167 Hannover, Germany*

<sup>3</sup>*Center for Computational Relativity and Gravitation, Rochester Institute of Technology,  
170 Lomb Memorial Drive, Rochester, New York 14623, USA*

<sup>4</sup>*Perimeter Institute for Theoretical Physics, Waterloo, ON N2L 2Y5, Canada*

<sup>5</sup>*Physics & Astronomy Department, University of Waterloo, Waterloo, ON N2L 3G1, Canada*

<sup>6</sup>*Center for Computation & Technology, Louisiana State University, Baton Rouge, LA 70803, USA*

(Dated: 2019-03-12)

We find strong numerical evidence for a new phenomenon in a binary black hole spacetime, namely the merger of marginally outer trapped surfaces (MOTSs). By simulating the head-on collision of two non-spinning unequal mass black holes, we observe that the MOTS associated with the final black hole merges with the two initially disjoint surfaces corresponding to the two initial black holes. This yields a connected sequence of MOTSs interpolating between the initial and final state all the way through the non-linear binary black hole merger process. In addition, we show the existence of a MOTS with self-intersections formed immediately after the merger. This scenario now allows us to track physical quantities (such as mass, angular momentum, higher multipoles, and fluxes) across the merger, which can be potentially compared with the gravitational wave signal in the wave-zone, and with observations by gravitational wave detectors. This also suggests a possibility of proving the Penrose inequality mathematically for generic astrophysical binary black hole configurations.

The merger of two black holes (BHs) is often visualized by an event horizon (EH), the boundary of the portion of spacetime causally disconnected from far away observers. An example of this is [34], showing the well known “pair of pants” picture of the EH for a binary black hole collision. However, EHs are not generally suitable for extracting quantities of physical interest and tracking them all the way through the merger in quantitative studies. In perturbative regimes or in cases when the end state of the EH is known, it is sometimes possible to use EHs to calculate mass, angular momentum, energy fluxes etc. [23], but this does not carry over to non-perturbative situations (such as during a binary black hole (BBH) merger) [8, 10, 20, 24].

It is much more satisfactory, both for conceptual and practical reasons, to use instead marginally trapped surfaces, first introduced by Penrose for proving the singularity theorems [36]. Let  $S$  be a closed 2-surface with in- and out-going future-directed null normals  $n^a$  and  $\ell^a$  respectively, and let  $\Theta_{(n)}$  and  $\Theta_{(\ell)}$  be the corresponding expansions. Trapped surfaces have  $\Theta_{(\ell)} < 0$ ,  $\Theta_{(n)} < 0$ , while a marginally outer trapped surface (MOTS) has  $\Theta_{(\ell)} = 0$  with no restriction on  $\Theta_{(n)}$ . The outermost MOTS on a given Cauchy surface, known as an apparent horizon (AH), has been used to locate BHs even in the earliest numerical BH simulations (see e.g. [42]). The presence of a trapped surface in a spacetime shows the presence of a singularity and an EH. MOTSs were thus used as proxies for EHs which are much harder to locate numerically.

Over the last two decades, however, it has become clear that MOTSs are much better behaved than previously expected. The world tube traced out by a MOTS during time evolution can be used to study energy fluxes, the evolution of mass, angular momentum and higher multipole mo-

ments [4, 18, 22, 28, 41]. The world tube can be used as an inner boundary for Hamiltonian calculations, and the laws of BH mechanics hold [8, 10, 12, 21, 25, 27, 29]. In general the world tubes can be null, spacelike, timelike, or of mixed signature [5–8, 11, 12]. In stationary spacetimes and in perturbative settings, these calculations coincide with expectations from EHs, but this framework is generally applicable.

Despite this progress, there remains a significant gap in our understanding. For a BBH merger it is routine to compute physical quantities for either the two separate initial BHs or for the common final BH. It is not clear if there should exist a relationship between the two regimes separated by the merger. Neither is it known whether there is a connected sequence of MOTSs which takes us from the two separated individual MOTSs to the final one. The existence of such a connected sequence would allow the possibility of tracing physical quantities all the way through the dynamical and non-linear merger process. These predictions could potentially be compared with calculations of gravitational wave (GW) signals in the wave-zone and eventually with observations of GWs, thus offering a unique probe of dynamical and non-linear gravity.

Another motivation for studying the merger of MOTSs is related to cosmic censorship and the Penrose inequality. In 1973, Roger Penrose proposed an inequality relating the area  $A$  of a BH horizon to the spacetime’s total ADM mass  $M_{ADM}$  [37]:

$$A \leq 16\pi M_{ADM}^2. \quad (1)$$

As originally formulated by Penrose, this inequality applies to a marginally trapped surface  $S$  formed during gravitational collapse (though there are examples of AHs which violate the inequality [9]). A proof of this inequality with-

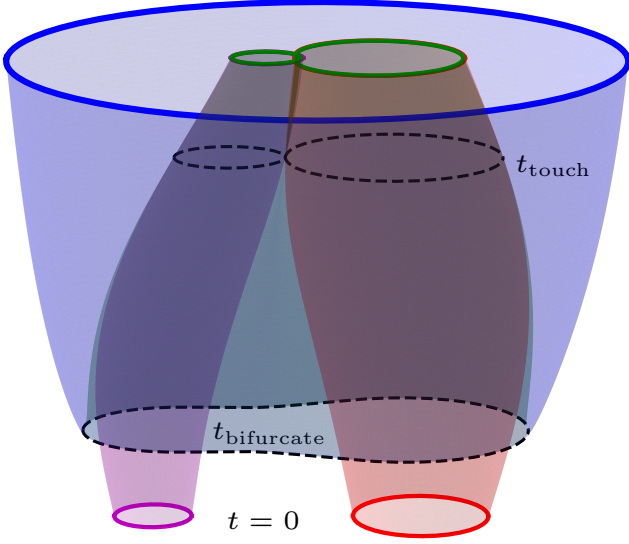


FIG. 1: The analog of the *pair-of-pants* picture for MOTSs from our numerical simulation. The tubes traced out by the individual MOTSs (colored red and purple) touch and penetrate each other. When the individual black holes get sufficiently close a common horizon is formed, which bifurcates into an inner branch (colored green) and an outer branch (colored blue). The outer branch settles down to the final equilibrium state, while the inner branch merges with the individual horizons precisely at the time when they touch.

out using event horizons is seen as strong support for cosmic censorship. Thus far, the inequality has been established rigorously for time symmetric initial data for an arbitrary number of BHs [13, 14, 26] (see [1, 15, 31, 33] for some alternate approaches, and [32] for a review). For a BBH system, the Penrose inequality implies

$$A_1 + A_2 \leq 16\pi M_{ADM}^2, \quad (2)$$

where  $A_{1,2}$  are the initial areas of the two individual BHs, taken to be two disjoint MOTSs  $\mathcal{S}_1$  and  $\mathcal{S}_2$ . Let  $\mathcal{S}_f$  be the final MOTS with area  $A_f$ . If there is a connected sequence of MOTSs which takes us from  $\mathcal{S}_{1,2}$  to  $\mathcal{S}_f$ , and if  $A_1 + A_2 \leq A_f$ , then this suggests an alternative route for a mathematical proof of the inequality for multiple BHs.

*Overview of results.*—We address this question by numerically simulating the head-on collision of two unequal mass black holes. A rendering of the numerical data from one of our simulations is shown in Fig. 1; this is the analog of the “pair of pants” picture for an event horizon. The world tubes traced out by the two individual MOTSs touch at a time  $t_{\text{touch}}$  and then penetrate each other. Sometime before  $t_{\text{touch}}$ , at  $t_{\text{bifurcate}}$ , the common horizon is formed and immediately bifurcates into an inner and outer branch. The outer branch approaches equilibrium as it loses its asymmetries. In contrast, the inner branch becomes increasingly distorted and merges with the individual MOTSs precisely

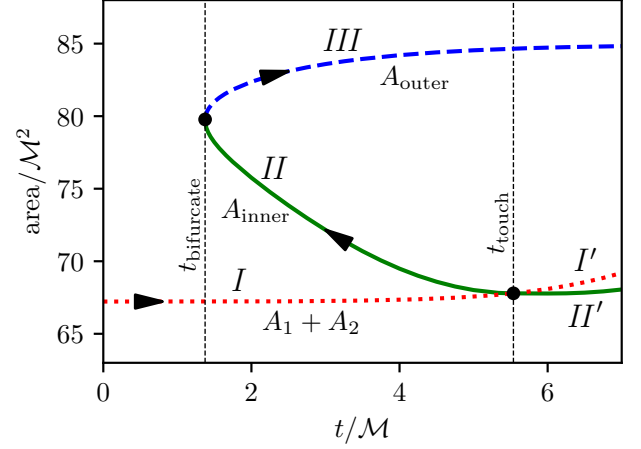


FIG. 2: The areas of the various MOTSs as functions of time for the same simulation shown in Fig. 1. The area of the AH is shown in blue, the inner common MOTS in green, and the sum of the areas of the individual MOTSs in red. Further details in text. Motivated by our choice of parameters, we measure in units of  $\mathcal{M} = M_{ADM}/1.3$ .

at the moment when they touch. Interestingly, as shall be detailed below, the inner branch still continues to exist after this merger, but it develops self-intersections, thereby providing evidence for topology change.

For the area increase and the Penrose inequality, also to be discussed further below, we follow the individual MOTSs up to the point when they touch, and then follow the common MOTS (initially backwards in time), eventually reaching the final equilibrium state of the outer MOTS. For the world tubes shown in Fig. 1, this leads to a plot of the area as a function of time shown in Fig. 2. We start with the two BHs far apart, represented by the MOTSs  $\mathcal{S}_1$  and  $\mathcal{S}_2$ , and track their areas  $A_1$  and  $A_2$ , respectively. The branch  $I$  and  $I'$  (dotted red) show  $A_1 + A_2$  which is always increasing;  $I$  and  $I'$  are respectively the portions before and after  $t_{\text{touch}}$ .

The common horizon is formed with a bifurcation into inner and outer portions  $\mathcal{S}_{\text{inner}}$  and  $\mathcal{S}_{\text{outer}}$  respectively, at the time  $t_{\text{bifurcate}}$ .  $\mathcal{S}_{\text{inner}}$  generates the branch  $II$  (solid green), which initially decreases in area and eventually merges with  $I$  at time  $t_{\text{touch}}$  (which also demarcates  $II$  and  $II'$ ). Segment  $III$  (dashed blue) is traced out by the AH which has increasing area and asymptotes to a final Schwarzschild or Kerr horizon. The required sequence of MOTSs is then  $I + II + III$  (segment  $II$  is traversed backwards in time); if we have monotonic area increase along this sequence, the Penrose inequality is guaranteed to hold. The portions  $I'$  and  $II'$  are not part of this sequence. Subtleties about the monotonicity of the area will be discussed further below.

*Methodology.*—Our main technical tool is a new method (and software) for locating MOTSs numerically which is

capable of finding even very highly distorted MOTSs [38–40]. This is a modification of the commonly used algorithm known as AHFinderDirect [44]. It was previously validated for sequences of time-symmetric initial data sets, and is here applied during a time evolution.

We use the Einstein toolkit [19, 30] infrastructure for our calculations. We set up initial conditions via the two-puncture single-domain method [3] and enforce axisymmetry following [39]. We solve the Einstein equations in the BSSN formulation as in [17], using a  $1 + \log$  slicing and a  $\Gamma$ -driver shift condition, with details of our initial and gauge conditions as described in [45].

We use 6th order finite differencing on a uniform grid spanning  $[0, 10] \times [0, 0] \times [-10, 10]$  and a 6th order Runge-Kutta time integrator. Most calculations shown here were performed with a resolution of  $h = 1/960$ . Additional resolutions were used to verify convergence. All parameter files are available in the repository [40].

*The merger of the inner horizons.*— We consider head-on collisions of non-spinning BHs starting with Brill-Lindquist (BL) initial data [16], representing a BBH system at a moment of time-symmetry. The bare masses of the two BHs are denoted  $(m_1, m_2)$  and  $d_0$  is the initial separation. While the Penrose inequality is known to hold in BL data [13, 14, 26], no such time symmetry is expected to occur in any astrophysical situation in our universe. Time symmetry implies that the two BHs approach each other and merge also under time reversal. Furthermore, the incoming radiation at past null-infinity mirrors the outgoing radiation at future null-infinity.

Some partial results on the behavior of  $\mathcal{S}_{\text{inner}}$  were known previously [22, 41]:  $\mathcal{S}_{\text{inner}}$  decreases rapidly in area initially and becomes increasingly distorted as it approaches  $\mathcal{S}_1$  and  $\mathcal{S}_2$ . With our new horizon finder, we are able to track  $\mathcal{S}_{\text{inner}}$  up to the merger point, and beyond. We present our results first for a particular initial configuration  $m_1 = 0.5$ ,  $m_2 = 0.8$  and  $d_0 = 1.3$ . We define  $\mathcal{M} = M_{\text{ADM}}/(m_1 + m_2) = M_{\text{ADM}}/1.3$ .

We have already shown the world tubes traced out by the MOTSs for this configuration in Fig. 1 and the areas in Fig. 2. The shapes of the various marginal surfaces at selected instants of time are shown in Fig. 3. The left panel shows the MOTSs after the AH has formed and  $\mathcal{S}_{\text{inner}}$  is fairly distorted. The center panel shows the MOTSs shortly before  $\mathcal{S}_{1,2}$  touch. The inset shows a close-up of the neck of  $\mathcal{S}_{\text{inner}}$ , which is very close to pinching off. The right panel shows the horizons at a later time when  $\mathcal{S}_{1,2}$  penetrate each other. The penetration of the individual MOTSs was first observed in [35, 43] (see also [2]). Interestingly,  $\mathcal{S}_{\text{inner}}$  still continues to exist at this time, but it is seen to develop self-intersections; Fig. 4 shows a close-up of the self-intersection. At later times  $\mathcal{S}_1$  and  $\mathcal{S}_2$  continue to move closer and the “knot” in  $\mathcal{S}_{\text{inner}}$  becomes bigger. We lose numerical resolution at later times when the horizons get too close to the punctures, and we have not attempted here to study the eventual fate of the inner horizons. It is suggested

in [35] that  $\mathcal{S}_{1,2}$  can cross the punctures and merge, though discontinuities are observed when the punctures cross the surfaces. These discontinuities might in fact hide further topology change as the punctures cross the MOTSs and could perhaps be resolved with our horizon finder.

We are led to conjecture that  $\mathcal{S}_{\text{inner}}$  has a cusp precisely at  $t_{\text{touch}}$ , and it coincides with  $\mathcal{S}_1 \cup \mathcal{S}_2$  at this time; the self-intersections develop immediately after  $t_{\text{touch}}$ . While numerical methods will likely not be able to precisely resolve the instant when the cusp is present, we can provide strong evidence that the time of the cusp formation coincides with  $t_{\text{touch}}$ . Fig. 5 shows various quantities which must all vanish at the point when  $\mathcal{S}_{1,2}$  touch. First, it shows the proper distance between  $\mathcal{S}_1$  and  $\mathcal{S}_2$  measured at facing points along the  $z$ -axis. Then we plot the proper circumference of the neck of  $\mathcal{S}_{\text{inner}}$ , and the proper distance between  $\mathcal{S}_{1,2}$  and  $\mathcal{S}_{\text{inner}}$  along the  $z$ -axis (the latter distances are scaled up by a factor of 10 to be properly visible on this plot). To define the “neck” for a self-intersecting MOTS, we look at all the curves of rotation obtained by starting with a point on the knot and rotating it around the symmetry axis. The neck is the curve which has smallest proper circumference. The dotted lines show the extrapolation to zero whence we see that, as far as we can tell,  $\mathcal{S}_{\text{inner}}$  pinches off at the same time (within  $\mathcal{O}(10^{-5})\mathcal{M}$ ) when  $\mathcal{S}_{1,2}$  touch, and the self-intersections occur immediately after  $t_{\text{touch}}$ .

*The area increase law.*— From Fig. 2, one might conclude that the area increases monotonically along the sequence  $I + II + III$  discussed earlier. A closer look near  $t_{\text{touch}}$  (see Fig. 6) reveals a small area *increase*  $\Delta A$  just prior to  $t_{\text{touch}}$ ; the area is *not* strictly monotonically increasing along the sequence  $I + II + III$ . The area of course does increase when we compare the final black hole with the sum of the initial areas, thus the Penrose inequality is valid. This result indicates that a mathematical proof using this route must necessarily address this behavior, and there might be important physical information hidden in this area increase.

We repeat the simulations for different mass ratios and initial separations. The values of  $\Delta A$  over a portion of the parameter space are shown in Fig. 7. The  $x$ -axis is the proper distance  $\tilde{d}_0$  between  $\mathcal{S}_{1,2}$  in units of the ADM mass, while the  $y$ -axis is the ratio of the irreducible masses  $M_{\text{irr}}^{(1,2)} := \sqrt{A_{1,2}/16\pi}$  of  $\mathcal{S}_{1,2}$ . The values of  $\Delta A$  are shown next to the points and also indicated by the size of the dots. The configurations within the shaded region are those which have the common AH already present in the initial data. For fixed mass-ratio,  $\Delta A$  decreases as  $\tilde{d}_0$  is increased, which suggests that astrophysical initial data may have vanishing  $\Delta A$ .

*Conclusions.*— We have studied the process by which two marginal surfaces merge to form a common final BH. This is similar to and complements the “pair of pants” picture of a BH merger using EHs. We have provided strong numerical evidence that there is a connected sequence of

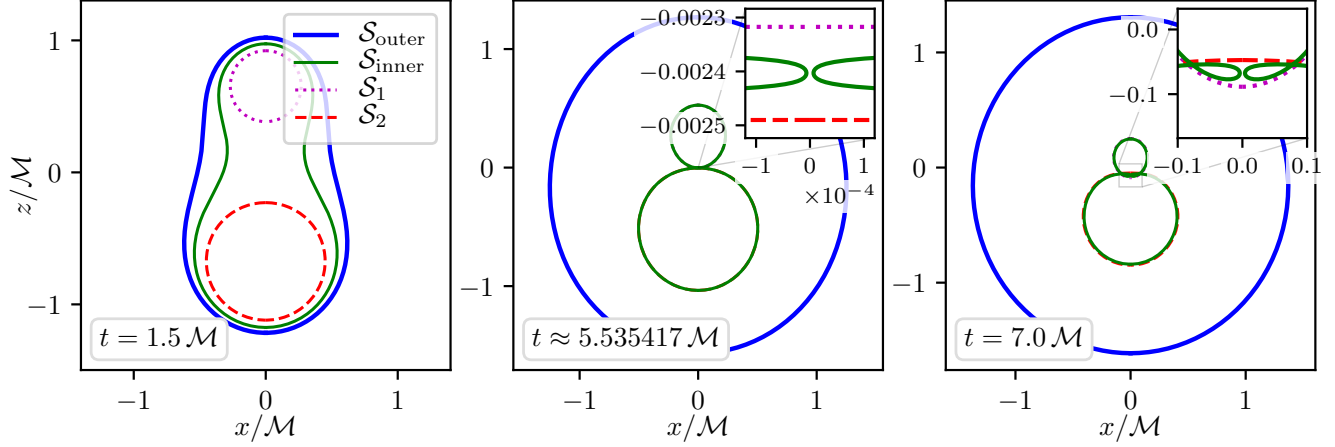


FIG. 3: The shapes of the horizons at various times in the simulation; this is the same simulation as shown in Figs. 1 and 2. The numerical values of  $t_{\text{touch}}$  and  $t_{\text{bifurcate}}$  are found to be  $t_{\text{touch}} \approx 1.374602 \mathcal{M}$  and  $t_{\text{bifurcate}} \approx 5.537818 \mathcal{M}$ , respectively. The left panel is about  $0.1254 \mathcal{M}$  after  $t_{\text{bifurcate}}$ , whereas the middle panel is about  $0.0024 \mathcal{M}$  before  $t_{\text{touch}}$ . The right panel is at the end of the simulation, well after  $t_{\text{touch}}$ .

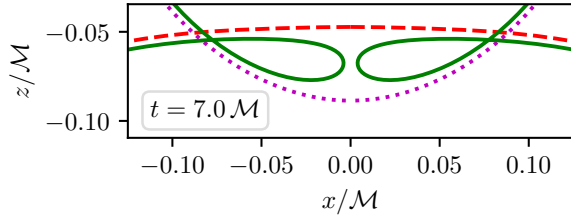


FIG. 4: A closer look at the self-intersection for the right panel in Fig. 3.

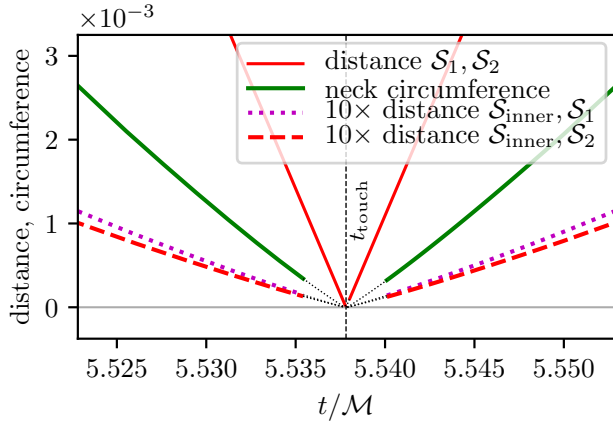


FIG. 5: Different measures showing the merger  $\mathcal{S}_{1,2,\text{inner}}$ .

marginal surfaces in this process. This will potentially allow us to track physical quantities through the merger and to compare with results obtained from gravitational waveforms. We find a new phenomenon, namely the formation

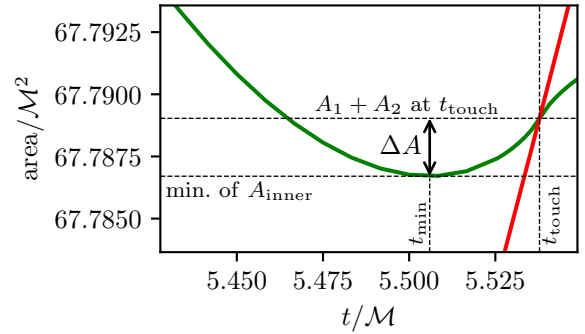


FIG. 6: A closer look at Fig. 2 near  $t_{\text{touch}}$  showing the anomalous area increase of  $\mathcal{S}_{\text{inner}}$ .

of MOTSs with self-intersections. Finally, this scenario suggests a different way of attacking the Penrose inequality. The area increase  $\Delta A$  of  $\mathcal{S}_{\text{inner}}$  just before the merger is still to be understood and, given the thermodynamic interpretation of the area, this may contain useful physical information.

*Acknowledgments.*— We thank Lars Andersson, Abhay Ashtekar, Alex Nielsen, Jeff Winicour, Jose-Luis Jaramillo and the referees for valuable discussions and suggestions. O.B. acknowledges the National Science Foundation (NSF) for financial support from Grant No. PHY-1607520. This research was also supported by the Perimeter Institute for Theoretical Physics. Research at Perimeter Institute is supported in part by the Government of Canada through the Department of Innovation, Science and Economic Development Canada and by the Province of Ontario through the Ministry of Economic Development, Job Creation and

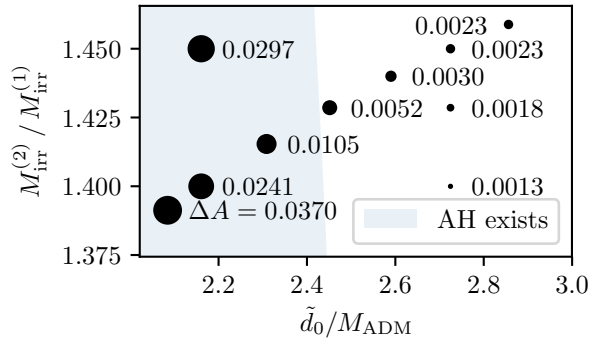


FIG. 7: Area increases for various initial conditions. See text for details.

Trade. Some calculations were performed on the *Niagara* cluster of the University of Toronto.

- [1] S. Alexakis. The Penrose inequality on perturbations of the Schwarzschild exterior. 2015.
- [2] L. Andersson, M. Mars, J. Metzger, and W. Simon. The time evolution of marginally trapped surfaces. *Classical and Quantum Gravity*, 26(8):085018, apr 2009.
- [3] M. Ansorg, B. Brügmann, and W. Tichy. A single-domain spectral method for black hole puncture data. *Phys. Rev. D*, 70:064011, 2004.
- [4] A. Ashtekar, M. Campiglia, and S. Shah. Dynamical Black Holes: Approach to the Final State. *Phys. Rev.*, D88(6):064045, 2013.
- [5] A. Ashtekar et al. Isolated horizons and their applications. *Phys. Rev. Lett.*, 85:3564–3567, 2000.
- [6] A. Ashtekar and B. Krishnan. Dynamical horizons: Energy, angular momentum, fluxes and balance laws. *Phys. Rev. Lett.*, 89:261101, 2002.
- [7] A. Ashtekar and B. Krishnan. Dynamical horizons and their properties. *Phys. Rev.*, D68:104030, 2003.
- [8] A. Ashtekar and B. Krishnan. Isolated and dynamical horizons and their applications. *Living Rev. Rel.*, 7:10, 2004.
- [9] I. Ben-Dov. The Penrose inequality and apparent horizons. *Phys. Rev.*, D70:124031, 2004.
- [10] I. Booth. Black hole boundaries. *Can. J. Phys.*, 83:1073–1099, 2005.
- [11] R. Bousso and N. Engelhardt. New Area Law in General Relativity. *Phys. Rev. Lett.*, 115(8):081301, 2015.
- [12] R. Bousso and N. Engelhardt. Proof of a New Area Law in General Relativity. *Phys. Rev.*, D92(4):044031, 2015.
- [13] H. L. Bray. Proof of the riemannian penrose inequality using the positive mass theorem. *J. Differential Geom.*, 59(2):177–267, 10 2001.
- [14] H. L. Bray and P. T. Chrusciel. The Penrose inequality. 2003.
- [15] H. L. Bray and H. P. Roesch. Null Geometry and the Penrose Conjecture. 2017.
- [16] D. R. Brill and R. W. Lindquist. Interaction energy in geometrostatics. *Phys. Rev.*, 131:471–476, 1963.
- [17] J. D. Brown, P. Diener, O. Sarbach, E. Schnetter, and M. Tiglio. Turduckening black holes: an analytical and computational study. *Phys. Rev. D*, 79:044023, 2009.
- [18] O. Dreyer, B. Krishnan, D. Shoemaker, and E. Schnetter. Introduction to Isolated Horizons in Numerical Relativity. *Phys. Rev.*, D67:024018, 2003.
- [19] Einstein Toolkit: Open software for relativistic astrophysics. <http://einstein toolkit.org/>.
- [20] V. Faraoni and A. Prain. Understanding dynamical black hole apparent horizons. *Lecture Notes in Physics*, 907:1–199, 2015.
- [21] E. Gourgoulhon and J. L. Jaramillo. A 3+1 perspective on null hypersurfaces and isolated horizons. *Phys. Rept.*, 423:159–294, 2006.
- [22] A. Gupta, B. Krishnan, A. Nielsen, and E. Schnetter. Dynamics of marginally trapped surfaces in a binary black hole merger: Growth and approach to equilibrium. *Phys. Rev.*, D97(8):084028, 2018.
- [23] S. W. Hawking and J. B. Hartle. Energy and angular momentum flow into a black hole. *Commun. Math. Phys.*, 27:283–290, 1972.
- [24] S. A. Hayward. Black holes: New horizons. In *Recent developments in theoretical and experimental general relativity, gravitation and relativistic field theories. Proceedings, 9th Marcel Grossmann Meeting, MG’9, Rome, Italy, July 2–8, 2000. Pts. A–C*, pages 568–580, 2000.
- [25] S. A. Hayward. Energy and entropy conservation for dynamical black holes. *Phys. Rev.*, D70:104027, 2004.
- [26] G. Huiskens and T. Ilmanen. The inverse mean curvature flow and the riemannian penrose inequality. *J. Differential Geom.*, 59(3):353–437, 11 2001.
- [27] J. L. Jaramillo. An introduction to local Black Hole horizons in the 3+1 approach to General Relativity. *Int. J. Mod. Phys.*, D20:2169, 2011.
- [28] B. Krishnan. Fundamental properties and applications of quasi-local black hole horizons. *Class. Quant. Grav.*, 25:114005, 2008.
- [29] B. Krishnan. Quasi-local black hole horizons. In A. Ashtekar and V. Petkov, editors, *Springer Handbook of Spacetime*, pages 527–555. Springer-Verlag, 2014.
- [30] F. Löffler, J. Faber, E. Bentivegna, T. Bode, P. Diener, R. Haas, I. Hinder, B. C. Mundim, C. D. Ott, E. Schnetter, G. Allen, M. Campanelli, and P. Laguna. The Einstein Toolkit: A Community Computational Infrastructure for Relativistic Astrophysics. *Class. Quantum Grav.*, 29(11):115001, 2012.
- [31] M. Ludvigsen and J. A. G. Vickers. An inequality relating total mass and the area of a trapped surface in general relativity. *Journal of Physics A: Mathematical and General*, 16(14):3349–3353, oct 1983.
- [32] M. Mars. Present status of the Penrose inequality. *Class. Quant. Grav.*, 26:193001, 2009.
- [33] M. Mars and A. Soria. On the Penrose inequality along null hypersurfaces. *Class. Quant. Grav.*, 33(11):115019, 2016.
- [34] R. A. Matzner, H. E. Seidel, S. L. Shapiro, L. Smarr, W. M. Suen, S. A. Teukolsky, and J. Winicour. Geometry of a black hole collision. *Science*, 270:941–947, 1995.
- [35] P. Mösta, L. Andersson, J. Metzger, B. Szilágyi, and J. Winicour. The Merger of Small and Large Black Holes. *Class. Quant. Grav.*, 32(23):235003, 2015.
- [36] R. Penrose. Gravitational collapse and space-time singular-

- ities. *Phys. Rev. Lett.*, 14:57–59, 1965.
- [37] R. Penrose. Naked singularities. *Annals N. Y. Acad. Sci.*, 224:125–134, 1973.
  - [38] D. Pook-Kolb, O. Birnholtz, B. Krishnan, and E. Schnetter. Existence and stability of marginally trapped surfaces in black-hole spacetimes. *Phys. Rev. D*, 99:064005, Mar 2019.
  - [39] D. Pook-Kolb, O. Birnholtz, B. Krishnan, and E. Schnetter. Self-intersecting marginally outer trapped surfaces. 2019.
  - [40] D. Pook-Kolb, O. Birnholtz, B. Krishnan, E. Schnetter, and V. Zhang. MOTS Finder version 1.3, July 2019.
  - [41] E. Schnetter, B. Krishnan, and F. Beyer. Introduction to dynamical horizons in numerical relativity. *Phys. Rev.*, D74:024028, 2006.
  - [42] L. Smarr, A. Čadež, B. DeWitt, and K. Eppley. Collision of two black holes: Theoretical framework. *Phys. Rev. D*, 14:2443–2452, Nov 1976.
  - [43] B. Szilagyi, D. Pollney, L. Rezzolla, J. Thornburg, and J. Winicour. An Explicit harmonic code for black-hole evolution using excision. *Class. Quant. Grav.*, 24:S275–S293, 2007.
  - [44] J. Thornburg. Finding apparent horizons in numerical relativity. *Phys. Rev. D*, 54:4899–4918, 1996.
  - [45] B. Wardell, I. Hinder, and E. Bentivegna. Simulation of GW150914 binary black hole merger using the Einstein Toolkit, Sept. 2016.